Hindawi
Adsorption Science & Technology
Volume 2022, Article ID 9884474, 17 pages
https://doi.org/10.1155/2022/9884474

Research Article

Removal of Reactive Black Dye in Water by Magnetic Mesoporous Carbon from Macadamia Nutshell

Sakonsupa Damdib,[1] Nuttamon Vanichsetakul,[1] Phanuwat Pimpapoat,[2] Sergey Mikhalovsky,[3,4] Rosa Busquets,[5] Adisak Siyasukh,[6,7] and Nattaporn Tonanon[1]

[1]*Bio-Circular-Green economy Technology and Engineering Center (BCGeTEC), Department of Chemical Engineering, Faculty of Engineering, Chulalongkorn University, Bangkok 10330, Thailand*
[2]*Pong Yaeng Agriculture Company Limited-V.P.C. Group (PY-VPC), 50 Soi Tiantalae 20-Yak 7, Bangkhuntian-Chaitalae Rd., Samaedum, Bangkhuntian, Bangkok 10150, Thailand*
[3]*Advanced Nanostructured Materials Design and Consultancy (ANAMAD) Limited, Sussex Innovation Centre, University of Sussex, Science Park Square, Falmer, BN1 9SB Brighton, UK*
[4]*Chuiko Institute of Surface Chemistry, Kyiv, Ukraine*
[5]*School of Life Sciences, Pharmacy and Chemistry, Kingston University London, Kingston Upon Thames, KT1 2EE Surrey, UK*
[6]*Research Laboratory of Pollution Treatment and Environmental Material (PTEM), Department of Industrial Chemistry, Faculty of Science, Chiang Mai University, Chiang Mai 50200, Thailand*
[7]*Materials Science Research Center, Faculty of Science, Chiang Mai University, Chiang Mai 50200, Thailand*

Correspondence should be addressed to Nattaporn Tonanon; nattaporn.t@chula.ac.th

Received 11 August 2022; Revised 15 November 2022; Accepted 22 November 2022; Published 6 December 2022

Academic Editor: Senthil Kumar Ponnusamy

The novel and intriguing role of $Fe(NO_3)_3$ as a chemical activator in carbonization of macadamia nutshell is introduced in this work. Magnetic mesoporous carbon was achieved by chemical activation of macadamia nutshell with $Fe(NO_3)_3$ under nitrogen atmosphere at 850°C (MMC-850). Porosity of MMC-850 included S_{BET} 317 m^2/g with V_{micro} 0.0796 cm^3/g and considerably high V_{meso} 0.4318 cm^3/g. Not only did MMC-850 possesses good magnetic properties with saturation magnetization and coercive force of 31.48 emu/g and 506.6 O_e, respectively, but MMC-850 also showed high-removal efficiency of reactive black dye (RB5) with maximum adsorption capacity at 123.51 mg/g. The experimental data fit the Langmuir isotherm and Elovich model. Thermal regeneration was effective in degrading RB5 and removal ability was above 90% after two regeneration cycles. RB5 removal from water by MMC-850 as an adsorbent is considered a facile and inexpensive method since macadamia nutshell is a food by-product which is a green and renewable carbon precursor. MMC-850 is a potential adsorbent because it can be separated from wastewater treatment system using magnetic force. Besides, MMC-850 particle is not brittle compared to other porous biochar/activated carbon with similar size; therefore, it is an excellent candidate for column packing or scaling up for wastewater treatment facilities in the future.

1. Introduction

Water pollution and water shortages are major global crises caused by expansion of the industrial sectors and rise of population [1]. Textile industries consume a large amount of water and chemicals [2, 3]. Reactive black 5 (RB5) is an azo dye which is one of the most widely used dye in textile industries due to its bright color and good colorfastness [4, 5]. Approximately, 10-15 percent of RB5 dye is lost in effluent wastewater during dyeing and finishing process [6, 7]. Since RB5 has intense dark hue, a minute amount of RB5 tremendously disturbs water clarity. In addition, chromophores in azo dyes cause mutagenicity and carcinogenicity in humans and animals [8, 9].

In general, there are several methods to remove dyes from wastewater, including physical or chemical processes

such as coagulation-flocculation [10–12], membrane filtration [13, 14], ozonation [15], advanced oxidation process (e.g., photocatalysis, Fenton and photo-Fenton, electrochemical, and sonolysis) [16–20], as well as biological process like anaerobic/aerobic process [21–23], or activated sludge process [24]. Most dye removal processes are complicated, expensive, and environment unfriendly while biological processes are green but time-consuming. However, most reactive dyes especially RB5 are not biodegradable, resulting in poor removal efficiency by biological techniques [25]. Adsorption is one of the most acceptable processes for dye-contaminated water treatment due to its simplicity, high efficiency, and low investment [26, 27]. Activated carbon is commonly used as an adsorbent due to its large surface area, high degree of microporosity, and desired surface functionalization [28]. Adsorption of RB5 in water with commercial-activated carbon and activated carbon prepared from coal, agricultural, and industrial wastes, including granular-activated carbon: FILTRASORB 400 [29], granular-activated carbon: DARCO®, granular-activated carbon: Norit® PK 1-3 [30], powdered-activated carbon [31], and activated carbon from H_3PO_4-bamboo [29], activated H_3PO_4-sawdust [32], activated carbon from textile sludge [33], activated carbon from palm shell [34], and activated carbon from walnut wood [35] have been thoroughly studied. Generally, commercial-activated carbon with specific or tailor-made properties is rather expensive.

Renewable and sustainable agricultural by-products such as tree nut shells, coconut shells, peanut shells, and rice husks and straw mainly consist of lignocellulose (cellulose, hemicellulose, and lignin) [36–40]. Porous properties of activated carbon strongly depend on lignocellulosic composition of raw materials. Carbon precursor with high-lignin content tends to have high yield and large number of mesopores [41, 42]. There are several macadamia plantations located at high-altitude area in northern part of Thailand. Macadamia nutshell (MNS) with approximately 50% lignin content [37, 38] is a food by-product from macadamia nut-cracking process in which about 60-70% by weight of MNS is generated [43, 44]. Since MNS exhibits unique properties such as high carbon and lignin contents with excellent hardness [45] which are crucial for preparation of tailor-made mesoporous carbon. Thus, MNS is a promising carbon precursor for adsorbents used in practical application such as column packing for scale up in the future.

In general, physicochemical properties of porous carbon (e.g., porous properties, functional groups, and magnetic properties) can be improved by physical activation (e.g., CO_2 and steam) or chemical activation (e.g., acids, alkali, oxidizing agents, and metal ions). Application of nitric acid (HNO_3) [46, 47], sodium hydroxide (NaOH) [46], phosphoric acid (H_3PO_4) [47], and sulfuric acid (H_2SO_4) [48] as chemical activators for carbonization of MNS were studied. In order to conveniently separate spent adsorbent from the system after wastewater treatment, magnetic adsorbents are considered to be attractive options. In general, magnetic porous carbon is obtained by impregnation of transition metal salts such as $FeSO_4{\cdot}nH_2O$ [49], $FeCl_3{\cdot}nH_2O$ [50, 51], $Fe(NO_3)_3{\cdot}nH_2O$ [52], $NiCl_2{\cdot}nH_2O$ [53], and $MnCl_2{\cdot}nH_2O$ [54] to carbon precursor. Unlike other iron compounds, $Fe(NO_3)_3$ creates not only good magnetic property but also high-mesopore volume. Effortless, green, sustainable, and economical ways of RB5 removal by magnetic mesoporous carbon adsorbent is introduced for the first time in this work.

2. Materials and Methods

2.1. Materials and Chemicals. Macadamia nutshell (MNS) was collected from Pong Yang agriculture, Chiang Mai, Thailand. Iron (III) nitrate nonahydrate ($Fe(NO_3)_3{\cdot}9H_2O$, (KemAus, ≥98%) was used. The commercial adsorbent was a granular-activated carbon (CAC) derived from bituminous coal, purchased from CARBOKARN Company Limited (I_2 number 1000). The anionic dyes, reactive black 5 (RB5, Sigma-Aldrich, >50%), were purchased from Sigma-Aldrich. Molecular structure of RB5 is shown in Figure 1.

2.2. Preparation of Magnetic Mesoporous Carbon (MMC) and Macadamia Nutshell Carbon (MNSC). Macadamia nutshell (MNS) was immersed in 0.1 M of $Fe(NO_3)_3$ and continuously stirred at 80°C for 2 hours, followed by oven drying at 80°C for 24 hours. Magnetic mesoporous carbons (MMCs) were fabricated by the carbonization under nitrogen atmosphere. Immersed macadamia nutshells were carbonized at 650°C and 850°C with a heating rate of 10°C/min with 2-hour holding time. Macadamia nutshell carbon (MNSC) was carbonized without chemical activation at 850°C. The samples were denoted as MMC-650, MMC-850, and MNSC-850, as listed in Table 1.

Remark: NR: no report.

2.3. Characterization. Surface area and pore volume were investigated by N_2 adsorption-desorption apparatus at 77 K (Autosorb-1-MP, Quantachrome). Morphology and surface features were demonstrated via scanning electron microscopy/energy dispersive X-ray spectroscopy (SEM, Hitachi S-3700 N). Crystalline structure and phase transformation were analyzed by powder X-ray diffraction with an X-ray diffractometer (D8 Advance, Bruker). Magnetic properties of magnetic porous carbon were studied by vibrating sample magnetometer (VSM; model-73098, Lank Shore). Iron content was determined by atomic absorption spectrophotometer (AAS; Analytik Jena ZEEnit 700P). The point of zero charge (pH_{pzc}) was determined by pH drift method [55].

2.4. Adsorption Experiments. Adsorption was performed in batch experiment. Firstly, for each carbon, 50 mg of sample was added to 100 mL of RB5 solution with different concentrations in the range of 5-300 mg/L. The mixtures were shaken at 200 rpm at 30°C until the appropriate time was reached. The concentration of RB5 was measured by an ultraviolet-visible spectrophotometer at maximum absorbance wavelength of 599 nm. The effect of pH on RB5 removal was performed in the range of pH3 to 11, adjusted by a buffer solution of acetic acid/sodium acetate and ammonium hydroxide/ammonium chloride at an initial concentration of 100 mg/L. Further, the stability of the

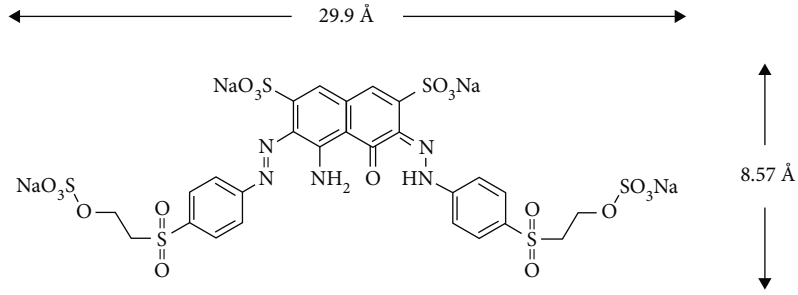

Figure 1: Molecular structure of the reactive black 5.

Table 1: Synthesis conditions of samples.

Samples	Raw material	Chemical activation	Carbonization temperature (°C)
MNSC-850	Macadamia nutshell	No	850
MMC-650	Macadamia nutshell	0.10 M $Fe(NO_3)_3$	650
MMC-850	Macadamia nutshell	0.10 M $Fe(NO_3)_3$	850
Commercial grade	Bituminous coal	No	NR

adsorbent after RB5 adsorption was studied. The amounts of adsorbed RB5 at equilibrium (q_e) were calculated by Equation (1)

$$q_e = \frac{(C_0 - C_e)V}{W}. \quad (1)$$

The removal percentage of RB5 was expressed by Equation (2)

$$\%\text{removal} = \frac{(C_0 - C_e)}{C_0} \times 100, \quad (2)$$

where C_0 is the initial concentrations of RB5 (mg/L) and C_e is the equilibrium concentrations of RB5 (mg/L); V is the solution volume (L) and W are the weight of adsorbent (g).

2.4.1. Adsorption Isotherm Model. Adsorption isotherm is used to describe the phenomena that occur during transportation of adsorbate in bulk solution to the adsorbent surface at a constant temperature and pH. Moreover, the maximum adsorption capacity as well as adsorption mechanisms that involve the interaction between adsorbate and adsorbent at adsorption equilibrium was described [56, 57]. Langmuir, Freundlich, and Dubinin-Radushkevich (D-R) models were used for data analysis.

Langmuir model is used for monolayer adsorption on an equivalent surface site with an equal sorption activation energy of each molecule, resulting in homogeneous adsorption [58]. Langmuir isotherm model is determined by Equation (3)

$$q_e = \frac{Q^0_{\max} b C_e}{1 + bC_e}, \quad (3)$$

where $Q^0{}_{\max}$ is the maximum monolayer adsorption capacity (mg/g), q_e is the amount of RB5 uptake at equilibrium (mg/g), and b is a constant related to the affinity between an adsorbent and adsorbate (L/mg).

Freundlich model is an empirical equation based on assumption that the adsorption occurs on heterogeneous surfaces of adsorbent. Freundlich isotherm model [59] is calculated by Equation (4):

$$q_e = K_F C_e^n, \quad (4)$$

where q_e is the amount of RB5 uptake at equilibrium (mg/g), K_F is the Freundlich constant (mg/g)/(mg/L), and n is the intensity parameter (dimensionless), which the magnitude of the surface heterogeneity is indicated.

D-R model is a semiempirical equation that is generally applied for an explanation of adsorption mechanism with Gaussian energy distribution onto heterogeneous surfaces [57, 60]. D-R model is expressed as follows in Equations (5)–(7):

$$q_e = q_{\text{DR}} e^{-K_{\text{RD}}\varepsilon^2}, \quad (5)$$

$$\varepsilon = \text{RT} \ln\left(1 + \frac{1}{C_e}\right), \quad (6)$$

$$E = \frac{1}{\sqrt{2K_{\text{DR}}}}, \quad (7)$$

where q_{RD} is the adsorption capacity (mg/g), K_{RD} is a constant related to the adsorption energy (mol^2/kJ^2), ε is the Polanyi potential, E is the free energy adsorption (kJ/mol), R is the gas constant (J/mol K), and T is the temperature (K).

2.4.2. Kinetic Adsorption Model. The pseudo-first-order (PFO) model, the pseudo-second-order (PSO), and the Elovich model are the most widely applied to describe kinetic process of adsorption and to calculate kinetic constant.

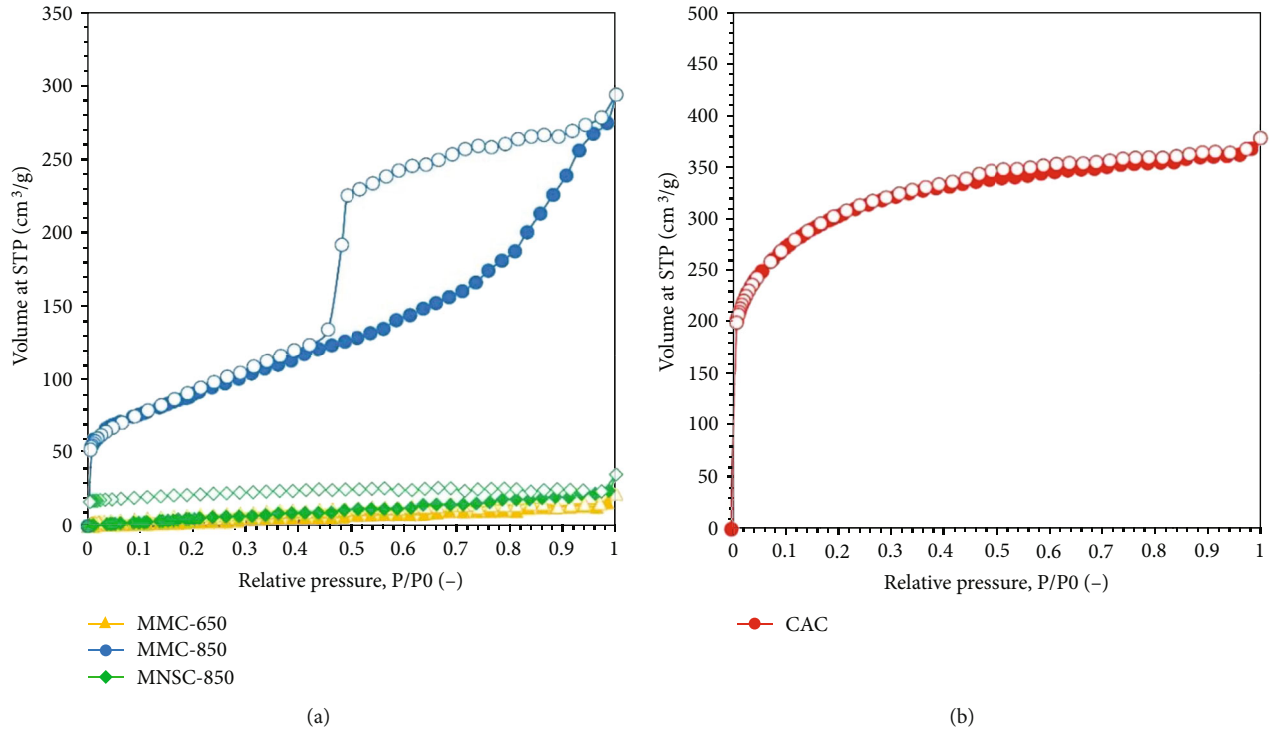

Figure 2: N_2 adsorption-desorption isotherms (77 K) of MMC-650, MMC-850, and MNSC-850 (a) and CAC (b).

Table 2: The specific surface area, total pore volume, micropore volume, and mesopore volume of MMC-650, MMC-850, MNSC-850, and CAC.

Samples	Type of isotherm	S_{BET} [m^2/g]	V_p [cm^3/g]	V_{micro} [cm^3/g]	V_{meso} [cm^3/g]
MMC-650	II	8	0.0010	0.0010	N/D
MMC-850	I+IV	317	0.4546	0.0796	0.4318
MNSC-850	II	49	0.0544	0.0047	N/D
CAC	I+IV	1103	0.5861	0.3040	0.1160

Remark: N/D: not determined.

The PFO rate expression by Lagergren [61] is presented in Equation (8)

$$q_t = q_e\left(1 - e^{-k_1 t}\right), \tag{8}$$

where q_{e1} and q_t are the amount of RB5 uptake at equilibrium and at any time (t) (mg/g), respectively; and k_1 is the PFO rate constant (1/min), and t is the time (min).

The PSO model [62] is determined by Equations (9) and (10)

$$q_t = \frac{q_e^2 k_2 t}{1 + k_2 q_e t}, \tag{9}$$

$$h = k_2 q_e^2, \tag{10}$$

where q_{e2} and q_t are the amount of RB5 uptake at equilibrium and at any time t (mg/g), respectively; k_2 is the rate constant of the PSO equation (g/mg·min), h is the initial rate constant (mg/g·min).

Elovich model is widely used to evaluate chemisorption [63, 64] indicated by Equation (11)

$$q_t = \frac{1}{\beta} \ln\left(1 + \alpha\beta t\right), \tag{11}$$

where q_t is the amount of RB5 uptake at any time t (mg/g), respectively; α is the initial rate constant (mg/g·min). β is the desorption constant during any one experiment (mg/g).

Meanwhile, intraparticle diffusion (IPD) model is often used to describe the mechanism of diffusion process and to predict the rate-limiting step of the adsorption process [65]. The adsorption dynamics can be explained by the following three steps: (1) film or surface diffusion of solute from the bulk solution through to the external surface of adsorbent, (2) transportation of solute into the interior of adsorption (intraparticle or pore diffusion), and (3) adsorption on the interior surface of the adsorbent [66–68]. The

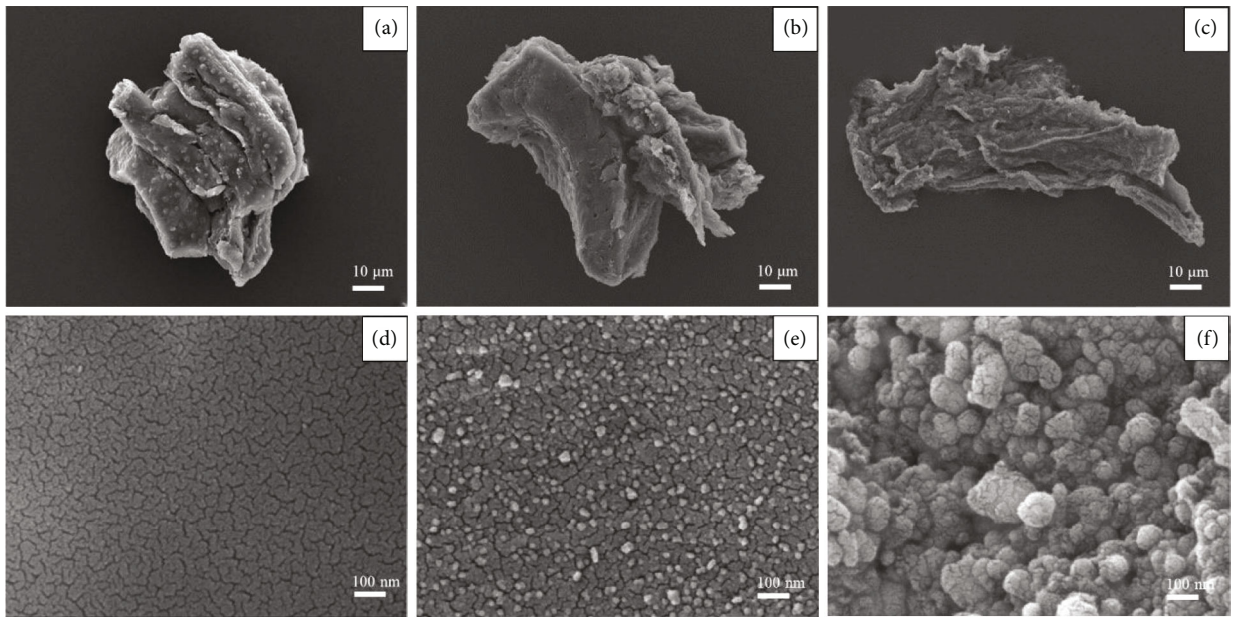

Figure 3: Scanning electron microscope (SEM) images of MNSC-850 (a, d), MMC-650 (b, e), and MMC-850 (c, f).

last step is rapid, so it was not considered a rate-limiting step. The IPD model [69] is calculated by Equation (12)

$$q_t = k_p\sqrt{t} + C, \tag{12}$$

where k_p is the rate constant of the intraparticle diffusion model (mg/g·min$^{1/2}$) and C is a constant associated with the thickness of the boundary layer (mg/g).

2.4.3. Thermodynamic Adsorption Models. The thermodynamic parameters of RB5 adsorption consisted of standard enthalpy change (ΔH^0), standard entropy change (ΔS^0), and standard Gibb's free energy change (ΔG^0). The relationship of $\Delta G\circ$ to $\Delta H\circ$ and $\Delta S\circ$ is described as follows:

$$\Delta G^0 = \Delta H^0 - T\Delta S^0. \tag{13}$$

These parameters can be estimated by the thermodynamic laws stated and the van't Hoff equation [55] in Equations (14)–(16)

$$\Delta G^0 = -\mathrm{RT}\ln K_c, \tag{14}$$

$$\ln K_c = -\left(\frac{\Delta H^0}{\mathrm{RT}}\right) + \frac{\Delta S^0}{R}, \tag{15}$$

$$K_c = \frac{\mathrm{bMW}_A}{\gamma_A} \times 55.5 \times 1000, \tag{16}$$

where 6 is dimensionless obtained by Langmuir constant (b); $\mathrm{MW_A}$ is molecular weight of RB5; γ_A is solution density; and the factor 55.5 is the number of moles of pure water per liter (1,000 g/L divided by 18 g/mol).

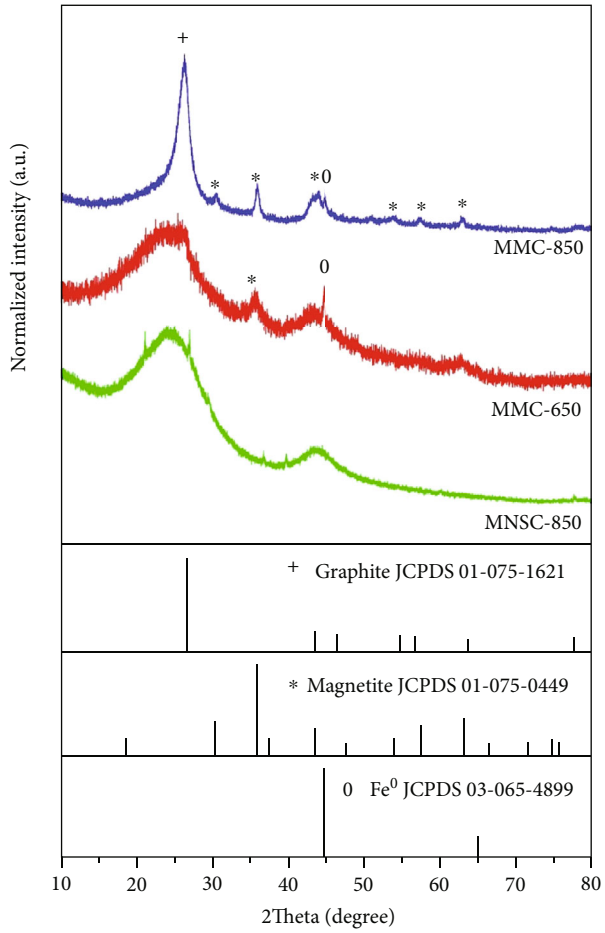

Figure 4: X-ray diffraction (XRD) patterns of MMC-850, MMC-650, and MNSC-850.

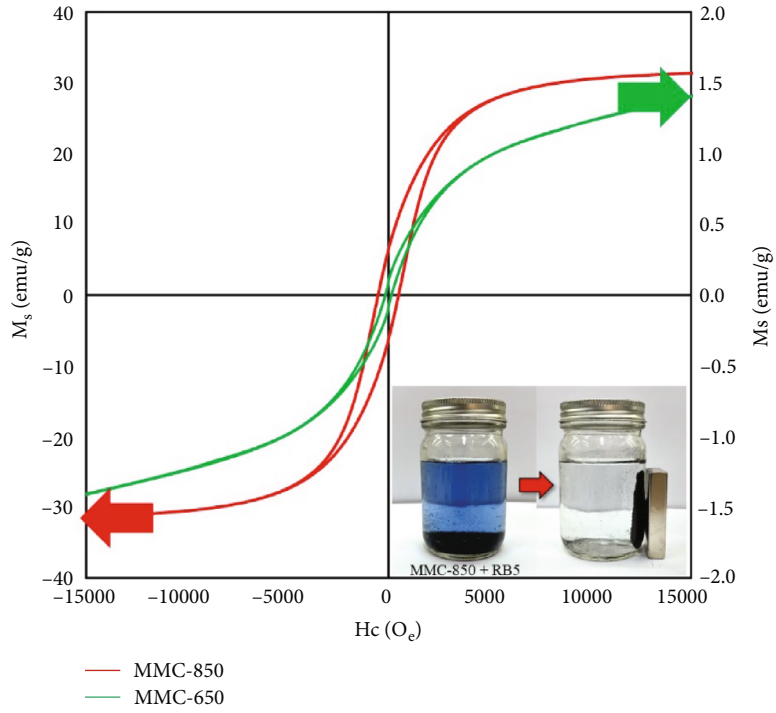

Figure 5: Vibrating sample magnetometer (VSM) curves of MMC-850 and MMC-650.

Table 3: Magnetic properties of MMC-650 and MMC-850 and chemical composition of all samples.

Samples	M_s (emu/g)	H_c (Oe)	Chemical composition					
			Atomic%			Weight%		
			C	O	Fe	C	O	Fe
MMC-650	1.49	149	87.37	7.38	5.28	92.97	5.87	1.21
MMC-850	31.48	506.6	72.59	1.61	25.80	91.48	1.52	6.99
MNSC-850	—	—	92.32	7.68	—	94.12	5.88	—

3. Results and Discussion

3.1. Preparation of Magnetic Mesoporous Carbon and Macadamia Nutshell Carbon

3.1.1. Effect of $Fe(NO_3)_3$ and Carbonization Temperature on Porous Properties. Porous properties of all samples were investigated by nitrogen adsorption-desorption isotherms as shown in Figure 2(a). MMC-650 demonstrated type II isotherm according to the International Union of Pure and Applied Chemistry (IUPAC) classification [70, 71] indicating nonporous adsorption. While macadamia nutshell carbonized at 850°C (MMC-850), exhibits type I and type IV isotherms, which suggests a combination of microporous and mesoporous structure. On the contrary, MMC-650 and MNSC-650 shared type II isotherm. The BET surface area and pore volume of all samples are presented in Table 2. MMC-650 and MNSC-850 exhibited small surface area at approximately 8 m^2/g and 49 m^2/g, respectively. As for the MMC-850, high-mesopore volumes were obviously generated in carbon structure where specific surface area, micropore volume, and mesopore volume were 317 m^2/g, 0.0796 cm^3/g, and 0.4318 cm^3/g, respectively. The preliminary results suggested that $Fe(NO_3)_3$ chemical activator together with carbonization at 850°C were crucial factors in generating pores structure especially mesopores [72, 73].

3.1.2. Effect of $Fe(NO_3)_3$ on Surface Morphology. Surface morphologies of MNSC-850, MMC-650, and MMC-850 are presented in Figure 3. Surface morphologies of MNSC-850, MMC-650, and MMC-850 were totally different. SEM micrographs clearly emphasized the role of $Fe(NO_3)_3$ on the tremendous increase of surface area for MMC-650 and MMC-850 compared to MNSC-850.

3.1.3. Effect of $Fe(NO_3)_3$ on Crystalline Arrangement and Phase Transformation. The crystalline arrangement and phase transformation of MMC-850, MMC-650, and MNSC-850 were determined from X-ray diffraction patterns, as shown in Figure 4. Both MMC-650 and MMC-850 exhibited peak at 2θ around 45°, which corresponded to metallic Fe (JCPDS no. 03-065-4899) [74, 75]. MNSC-850 and MMC-650 revealed broad diffraction peaks at 2θ around 26° and 44°, indicating amorphous carbon (low

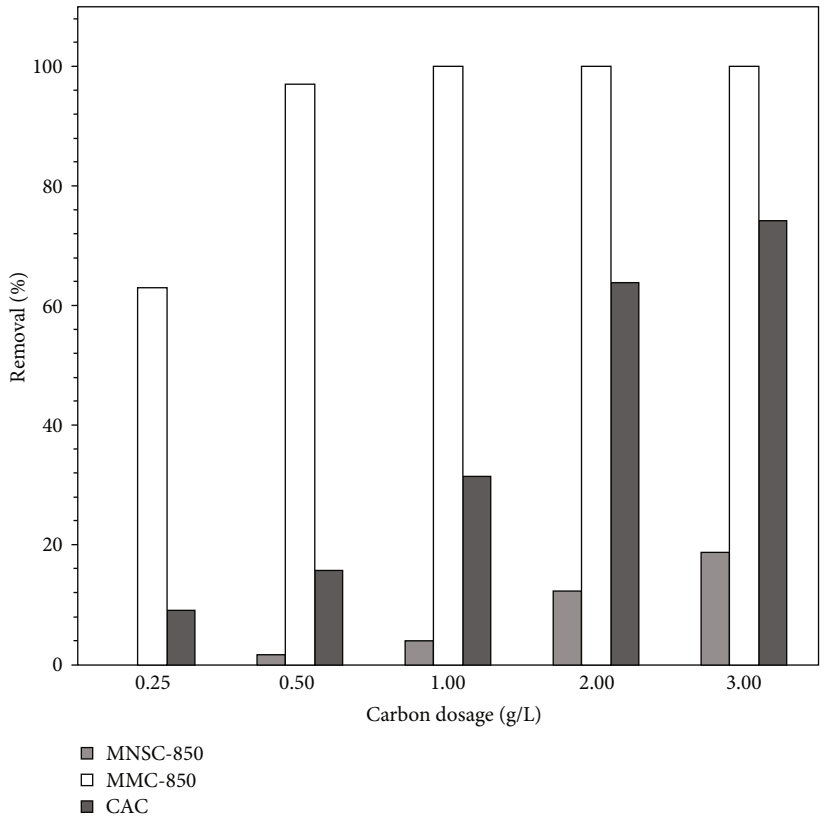

(a)

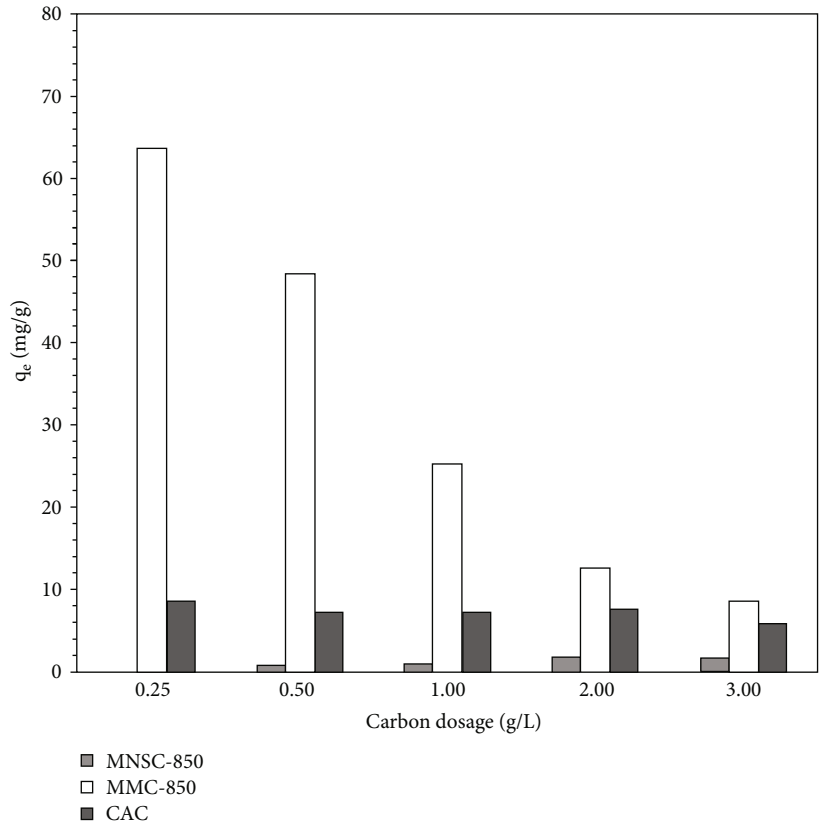

(b)

Figure 6: Effect of carbon dosage on RB5 removal (a) and adsorption efficiency (b) of MNSC-850, MMC-850, and CAC.

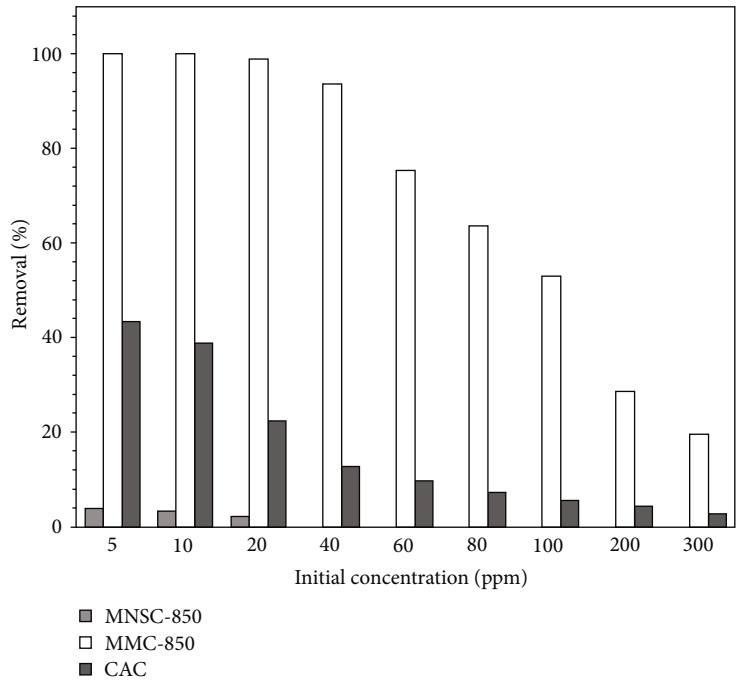

Figure 7: Effect of initial concentration on the adsorption of RB5 onto MNSC-850, MMC-850, and CAC.

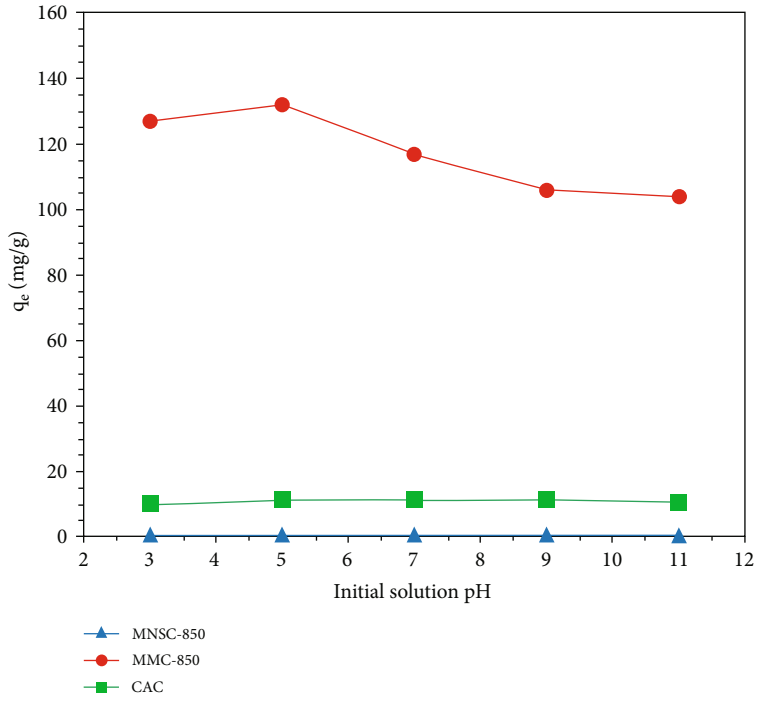

Figure 8: Effect of pH on the adsorption of RB5 solution onto MNSC-850, MMC-850, and CAC.

Table 4: Isotherm parameters of Langmuir, Freundlich, and D-R models for RB5 adsorption.

Sample	Langmuir			Freundlich			D-R		
	Q^0_{max} (mg/g)	K_L (L/mg)	R^2 (-)	K_f (mg/g)(L/mg)$^{1/n}$	n (-)	R^2 (-)	q_{DR} (mg/g)	E (kJ/mol)	R^2 (-)
MMC-850 (at 30°C)	123.51	0.64	0.9648	53.70	6.09	0.7696	$1.39E-04$	11.96	0.9072
MMC-850 (at 40°C)	102.29	0.55	0.9372	49.29	7.03	0.8459	$1.15E-04$	12.32	0.9675
MMC-850 (at 50°C)	105.25	0.46	0.9509	52.11	7.50	0.8681	$1.13E-04$	13.81	0.9535
CAC (at 30°C)	12.25	0.22	0.9915	5.28	5.82	0.8723	$1.34E-05$	12.02	0.9646

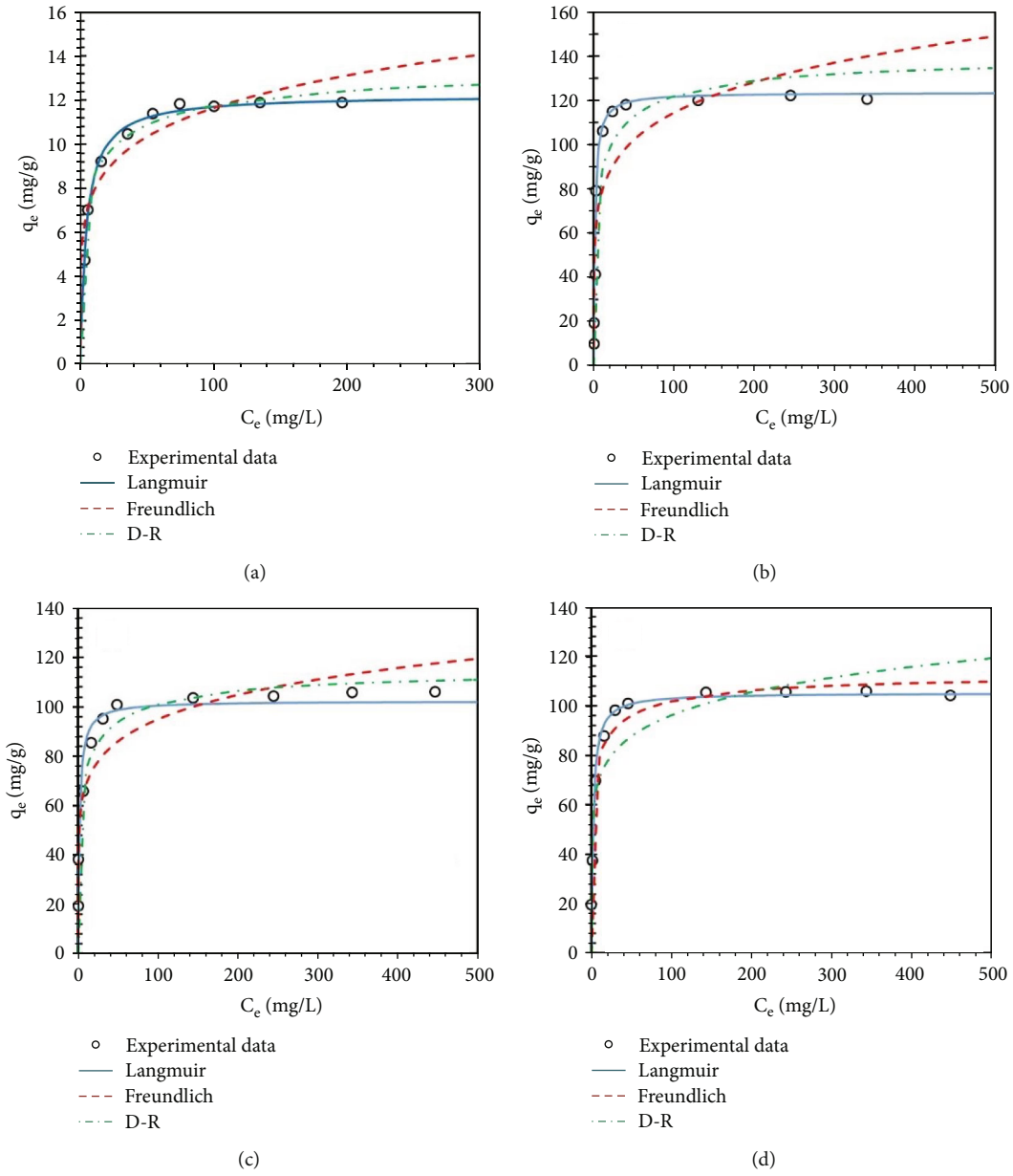

Figure 9: Adsorption isotherm models for RB5 adsorption onto (a) CAC, (b) MMC-850 at 30°C, (c) MMC-850 at 40°C, and (d) MMC-850 at 50°C.

graphitization degree) [76]. As regards MMC-850 presented a shape peak at 2θ around 26°, suggesting crystalline structure of graphite (JCPDS no. 01-075-1621). The presence of iron compounds in amorphous carbon at high temperatures can cause catalytic graphitization process, transformation of amorphous carbon into the graphitic structure [40]. Besides, only XRD pattern of MMC-850 demonstrated peaks at 2θ around 30.4°, 35.3°, 43.2°, 53.2°, 57.1°, and 62.6°, which corresponded to the characteristic peaks of magnetite (Fe_3O_4) (JCPDS no. 01-075-0499) [75]. Carbonization temperature of $Fe(NO_3)_3$ impregnated macadamia nutshell obviously played an important role for full formation of Fe_3O_4 phase. Complete magnetite phase was obtained when the suitable temperature (850°C) was reached.

Table 5: Thermodynamics parameter for RB5 adsorption onto MMC-850.

ΔH° (kJ/Mol)	ΔS° (kJ/mol K)	ΔG° (kJ/mol K)		
		30°C	40°C	50°C
-10.88	0.11	-43.79	-44.85	-45.94

3.1.4. Magnetic Properties of Magnetic Mesoporous Carbon. Magnetization curves of MMC-650 and MMC-850 are shown in Figure 5. The saturation magnetization (M_s) of MMC-650 was 1.493 emu/g, while the M_s of MMC-850 was up to 31.48 emu/g as shown in Table 3. It can be explained that the increase in carbonization temperature resulted in an increase in Fe_3O_4 content [72] corresponding

Table 6: Kinetic parameters of pseudo-first-order (PFO), pseudo-second-order (PSO), and Elovich model for RB5 adsorption.

Sample	Pseudo-first-order (PFO)			Pseudo-second-order (PSO)				Elovich		
	k_1 (min^{-1})	q_{e1} (mg/g)	R^2 (-)	k_2 (g/mg·min)	q_{e2} (mg/g)	h (mg/g·min)	R^2 (-)	α (mg/g·min)	β (mg/g)	R^2 (-)
MMC-850	0.0091	67.47	0.8628	0.0002	71.76	1.0260	0.9263	8.03	0.11	0.9753

to higher MS value. Furthermore, the magnetic hysteresis loop indicated ferromagnetic materials with a strong magnetic response to the external magnetic field [36, 77]. Consequently, it can easily be separated from aqueous solutions (as shown in the inset image of Figure 5). As a result, MMC can be recycled as an environmentally friendly adsorbent. In addition, SEM-EDS results were conducted to confirm the presence of iron compounds. From Table 3, the weight percentages of C, O, and Fe were 92.97, 5.87, and 1.21 for MMC-650 and 91.48, 1.52, and 6.99, respectively, for MMC-850. These results validated the presence of magnetite and metallic Fe in MMC-650 and MMC-850.

3.2. Adsorption of Reactive Black 5 Dye. The adsorption efficiency of MNSC-850, MMC-850, and CAC was investigated in batch adsorption tests. CAC was intentionally selected as an example of activated carbon adsorbents for general removal of organic contaminants in wastewater treatment process. Large specific surface area and high micropore volume of CAC are shown in Table 2.

3.2.1. Effect of Carbon Dosage on RB5 Removal and Adsorption Efficiency. RB5 adsorption efficiency was investigated using different amounts of carbon (0.25, 0.50, 1.0, 2.0, and 3.0 g/L) with an initial concentration of 20 mg/L at 30°C for 48 hours. In Figure 6, the more carbon dosage, the higher RB5 removal percentage (from 0.00 to 18.55 percent for MNSC-850, 63.04 to 99.99 for MMC-850, and 9.00 to 74.14 percent for CAC, respectively) becomes. In contrast, the adsorption capacity (q_e) of RB5 decreased while the dosage of adsorbents increased (from 1.56 to 0.00 mg/g for MNSC-850, 63.69 to 8.41 mg/g for MMC-850, and 8.46 to 5.80 mg/g for CAC, respectively) [37]. The results preliminarily suggest that mesoporous structure played a key role in RB5 adsorption from the aqueous solution. At carbon dosage of 3.0 g/L, commercial-activated carbon (CAC) provided a removal percentage of 74.14, despite the large specific surface area and large micropore structure (small mesopore structure). MMC-850 with a large mesopore structure showed high performance for RB5 removal, which was 97.04% at 0.50 g/L adsorbent. Therefore, adsorption experiment would be conducted with 0.5 g/L carbon dosage of MMC-850 for the rest of this study because of high-removal percentage (97.04 percent), and reasonable q_e value (48.35 mg/g).

3.2.2. Effect of Initial Concentration on the RB5 Removal. Effect of initial concentration on RB5 removal percentage was examined by initial concentration in the range of 5 to 300 mg/L, 0.5 g/L carbon dosage for 72 hours. Figure 7 shows that MNSC-850 had poor removal efficiency (from 4.04 to 0.00 percent), while MMC-850 and CAC showed decreases in the uptake of RB5 as the initial concentration increased (from 99.99 to 19.44 percent for MMC-850 and 43.52 to 2.81 for CAC). When the ratio between RB5 and active site on adsorbent surface is high as a result the removal percentage was decreased. The greater removal percentage at all concentrations and higher removal efficiency of MMC-850 compared to CAC were presumably due to the number of mesopores in MMC-850.

3.2.3. Effect of Adsorption pH on the RB5 Removal. The adsorption pH is an important factor in determining the surface charge of the adsorbent. Figure 8 shows the adsorption efficiency at pH range 3-11. MMC-850 under acidic conditions showed relatively high adsorption efficiency of 126.70 mg/g and 131.80 mg/g for pH 3 and pH 5, respectively. As the pH increased, the adsorption efficiency decreased due to the electrostatic interaction force. At adsorption pH < p H_{pzc} (6.8), the adsorbent surface was positively charged (protonation of acidic groups on the adsorbent surface [38]), and RB5 is negatively charged (deprotonate sulphonate groups; $-SO_3^-$ [39]); thus, affinity was formed between the adsorbent and the adsorbate through electrostatic interaction [41]. At pH > pH_{pzc}, adsorption efficiency is reduced due to repulsion between the negative charge on the adsorbent surface and RB5. Furthermore, RB5 adsorption efficiency of CAC and MNSC-850 was slightly changed with pH, approximately 11.13 mg/g for CAC and 0.58 mg/g for MNSC-850, respectively. Therefore, it can be concluded that the electrostatic interaction mechanism played insignificant role in RB5 adsorption [42].

3.2.4. Adsorption Equilibrium and Thermodynamics Adsorption. Table 4 displays parameters from Langmuir (Q^0_{max} and K_L), Freundlich (K_F and n), and D-R (q_{DR} and E) models and R^2 values. The experimental data of RB5 adsorption on MMC-850 at 30°C, 40°C, and 50°C were fitted with the Langmuir model, as shown in Figures 9(b)–9(d), and the coefficients of linear regression (R^2) were 0.9648, 0.9372, and 0.9509, respectively. CAC was also consistent with the Langmuir model (R^2 0.9915) at 30 C°. The results suggested a monolayer adsorption mechanism between the absorbent and the adsorbate.

D-R model can determine whether the adsorption mechanism was physisorption, ion exchange, or chemisorption through free energy of adsorption (E) calculations. Physisorption, ion-exchange adsorption, and chemisorption are represented by E values <8 kJ/mol, 8-16 kJ/mol, >16 kJ/mol, respectively [78]. In Table 4, the mean adsorption energy of MMC-850 was 11.96 kJ/mol, 12.32 kJ/mol, and 13.81 kJ/mol at 30°C, 40°C, and 50°C, respectively; whereas E of CAC was 12.02 kJ/mol at 30°C. The results showed that the

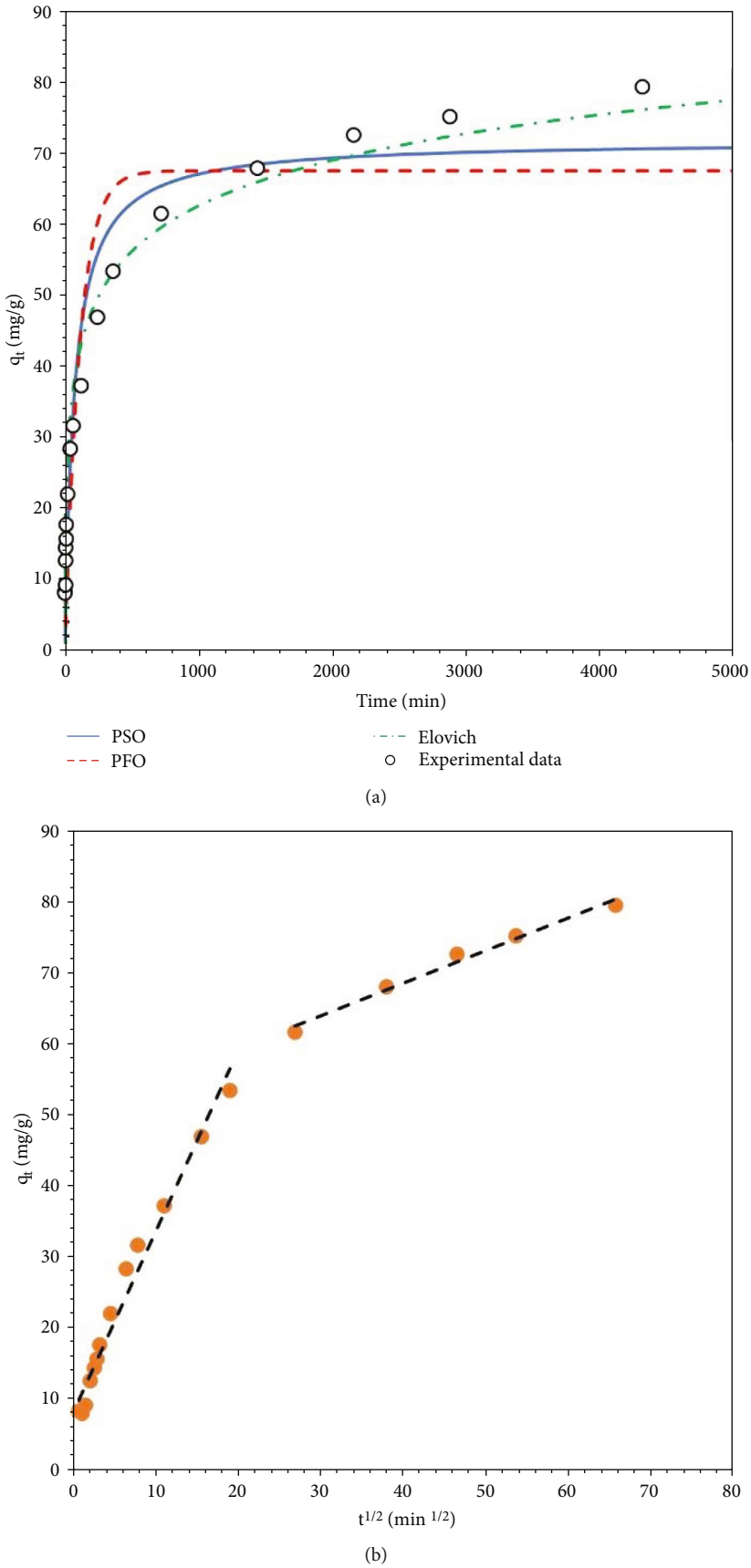

Figure 10: (a) Adsorption kinetic models for RB5 adsorption onto MMC-850; (b) intraparticle diffusion model for RB5 adsorption onto MMC-850.

Table 7: Intraparticle diffusion parameter for RB5 adsorption.

Sample	$K_{p,1}$ (mg/g·min$^{1/2}$)	C_1 (mg/g)	R^2 (-)	$K_{p,2}$ (mg/g·min$^{1/2}$)	C_2 (mg/g)	R^2 (-)
MMC-850	2.53	8.47	0.9757	0.46	50.16	0.9830

Table 8: Adsorbents for RB5 adsorption.

Adsorbents	Q^0 max (mg/g)	pH	Magnetic responsibility	Reference
Granular-activated carbon FILTRASORB 400 (F400)	197.50	NR	No	[29]
Granular-activated carbon Darco® 12x20, from lignite	348.00	10	No	[30]
Granular-activated carbon Norit® PK 1-3, from peat	394.00	10	No	[30]
Powdered-activated carbon (Merck)	58.82	NR	No	[31]
Activated carbons from bamboo	441.70	NR	No	[29]
Activated carbon from textile sludge	11.98	NR	No	[33]
Activated carbon from palm shell	25.12	2	No	[34]
Activated carbon from walnut wood	19.34	5	No	[35]
Activated carbon from *Acacia nilotica*	41.01	6.5	No	[81]
Magnetic-cellulose-PEI (MCPEI)	330.00	7	Yes	[82]
Magnetic iron oxide	18.00	NR	Yes	[83]
MMC-850	106.07	7	Yes	This work
CAC	12.25	7	No	This work

Remark: NR: no report.

adsorption mechanism of MMC-850 and CAC was an ion-exchange adsorption process.

The Langmuir model was used to calculate the maximum monolayer adsorption capacity (Q^0 max). MMC-850 and CAC had Q^0 max values of 123.51 mg/g and 12.25 mg/g at 30°C, respectively. The RB5 adsorption efficiency of MMC-850 (micropores and mesopores) was significantly higher than that of CAC (micropores without mesopores). The RB5 molecule has a dimension of 2.990 nm x 0.857 nm (Figure 1), which is larger than the micropore diameter (<2 nm), so the mesopores' role on RB5 adsorption cannot be overlooked [30]. The effect of temperature on RB5 adsorption was studied. The adsorption capacity of MMC-850 decreased as the temperature increased from 30 to 40°C, with Q^0 max values of 123.51 mg/g and 102.29 mg/g, respectively. Then, when the temperature increased from 40°C to 50°C, the adsorption efficiency did not significantly change. (from 102.29 to 105.25 mg/g).

Table 5 presents thermodynamics parameters for RB5 adsorption on MMC-850 at 30°C, 40°C, and 50°C. The negative value of ΔH° (-10.88 kJ/mol) suggested an exothermic adsorption process. Additionally, the type of adsorption was determined by ΔH°. The adsorption process was physical if ΔH° was less than 42 kJ/mol. However, ΔH° was higher than 42 kJ/mol implying the chemical adsorption process. The positive value of ΔS° indicated the increase in randomness at the adsorbent-adsorbate boundary during the adsorption process. Finally, the negative values of ΔG°

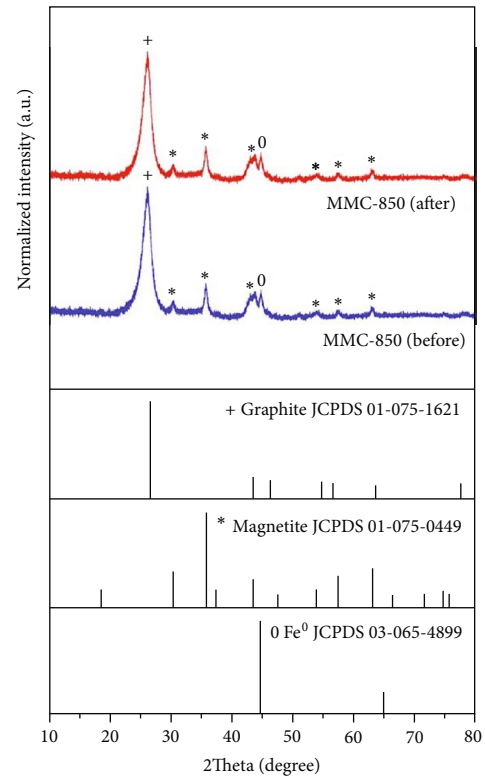

Figure 11: X-ray diffraction (XRD) patterns of MMC-850 before and after RB5 adsorption.

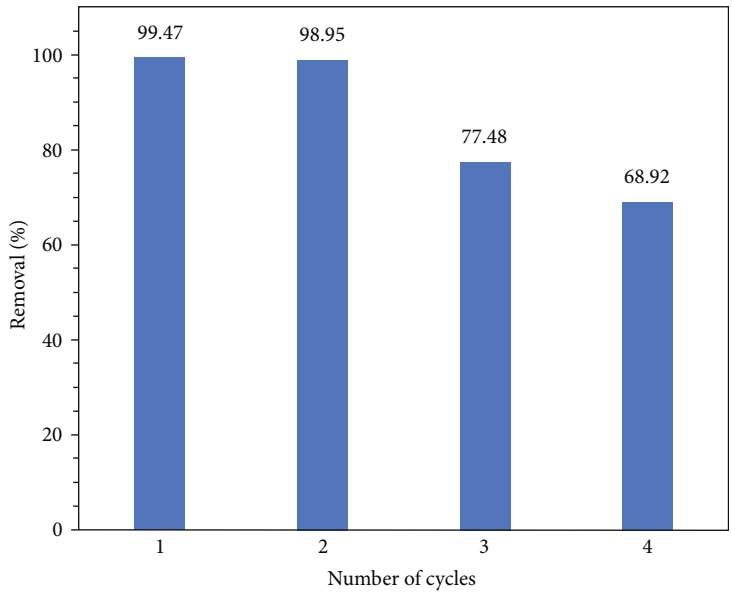

Figure 12: Thermal regeneration of RB5 onto MMC-850 at four cycles (condition: initial concentration 10 mg/L, carbon dosage 0.5 g/L, temperature 30°C, and time 72 hours.).

suggested that RB5 adsorption on MMC-850 was a spontaneous process at 30°C, 40°C, and 50°C.

3.2.5. Adsorption Kinetic of RB5. The adsorption kinetic and dynamic of RB5 on MMC-850 were investigated by kinetic rate models, pseudo-first-order (PFO), pseudo-second-order (PFO), and Elovich models. R^2 value and parameters calculated by the PFO (k_1 and q_{e1}), the PSO (k_2, qe_2, and h), and Elovich (α and β) model are listed in Table 6. A plot of the amount of RB5 adsorbed (mg/g) versus contact time at 100 mg/L and constant temperature of 30°C is presented in Figure 10(a). At the initial 1.0260 mg/g min adsorption rate (h), the amount of RB5 uptake (mg/g) increases with increasing contact time. In Figure 10(a), the experimental data was well-fitted with the Elovich model, with the R^2 value of 0.9745.

3.2.6. Intraparticle Diffusion Model. The intraparticle diffusion model is used for describing the adsorption mechanism and rate-limiting step. According to Weber and Morris [69]; when the regression of q_t versus $t^{1/2}$ is a straight line and passes through the origin, intraparticle diffusion is the rate-limiting step. Figure 10(b) reveals 2 straight lines, implying that adsorption occurred in two steps. The first and second steps were surface or film diffusion and adsorption, respectively. Although intraparticle diffusion was not the rate-limiting step, RB5 adsorption process was controlled by film diffusion and intraparticle diffusion [65]. R^2 value and other parameters (K_{id}, C) are listed in Table 7.

3.2.7. Adsorption Mechanisms of RB5 Adsorption. Mechanisms for cationic dye adsorption included electrostatic attraction, hydrogen bonding formation, $n-\pi$ interaction, pore filling, and $\pi-\pi$ interaction [30, 42, 79, 80]. MMC-850 was examined for changes in porosity properties after RB5 adsorption. Subsequently, the dominant mechanism of RB5 adsorption was pore filling, which was observed by the decrease in porosity. The V_{meso} of MMC-850 drastically decreased after RB5 adsorption (from 0.4318 to 0.1743 cm^3/g) as well as the S_{BET} (from 317 to 62.57 m^2/g), while V_{micro} was slightly reduced. (from 0.0796 to 0.0200 cm^3/g). This evidence supported the idea that mesopore structure plays a key role in RB5 adsorption. Therefore, it can be concluded that pore filling was dominant mechanism for RB5 adsorption.

From Section 3.2.3, RB5 adsorption efficiency of MMC-850 slightly changed when the solution pH changed. Therefore, it was suggested that the electrostatic interaction mechanism was negligible in RB5 adsorption. In addition, $\pi-\pi$ interactions between the aromatic ring in the RB5 structure, as shown in Figure 1, and C=C in the graphite structure was supported by prior studies in adsorption of RB5 onto activated carbon adsorbents and adsorption of methylene green (MG5) onto CAC (Norit RB4C) [30, 42].

3.2.8. MMC-850 as RB5 Adsorbent Compared to Others. RB5 adsorbents consisting of commercial-activated carbon, activated carbon from waste materials, and magnetic iron oxide as well as polyethyleneimine and cellulose on magnetic nanoparticles (MNPs) are listed in Table 8. However, carbon precursor of magnetic mesoporous carbon (MMC-850) is made from agricultural waste, providing them both inexpensive and renewable adsorbent. Besides, MMC-850 is considered as high potential as RB5 adsorbent in term of low cost, sustainability, facile, and green preparations by using only one $Fe(NO_3)_3$ chemical activator. Furthermore, RB5 adsorption by MMC-850 was conducted at pH 7 which is considered environment friendly process since no added chemical is required for pH adjustment. Moreover, MMC-850 can be easily separated from wastewater treatment afterward.

The future scale up of RB5 adsorption by MMC-850 by column packing is highly possible due to the strength of macadamia nutshell.

Remark: NR: no report.

3.3. Stability of Adsorbent after Adsorption Process. The stability of MMC-850 after RB5 adsorption was quantified by the amount of iron leached into solution during the adsorption process and crystalline structure of iron compounds in the adsorbent structure after the adsorption process. The result showed that the leaching content of iron was less than 0.50 mg/L in solution. Furthermore, the XRD patterns of MMC-850 after RB5 adsorption were identical to MMC-850 before RB5 adsorption, as illustrated in Figure 11. Therefore, magnetite and iron in the MMC-850 structure had negligible loss.

3.4. Thermal Regeneration of Spent Magnetic Mesoporous Carbon. The reversibility of adsorption was examined using a thermal regeneration experiment [84]. The spent magnetic mesoporous carbon was pyrolyzed under a nitrogen atmosphere at 400°C for 2 hours to decompose RB5 within the structure. For each cycle, the regenerated carbon was retested for adsorption efficiency at a RB5 concentration of 10 mg/L and 30°C. According to Figure 12, the removal percentage of RB5 decreased slightly from 99.47% in the first cycle to 98.95% in the second cycle. By the third cycle of the experiment, the RB5 removal percentage rapidly reduced to 77.48%, possibly due to a change in the pore structure within the absorbent material. At the end of the fourth cycle, the percentage of RB5 removed declined continuously from 77.48 to 68.92. It was observed that thermal regeneration was effective in degrading RB5.

4. Conclusion

Magnetic mesoporous carbon from macadamia nutshell (MMC-850) is a promising adsorbent in terms of facile preparation, low cost, and sustainability. $Fe(NO_3)_3$ and high-lignin content macadamia nutshell were carbonized at 850°C to generate magnetic mesoporous carbon that can be easily separated from RB5 adsorption system. It can be preliminarily concluded that mesopores on MMC-850 played a crucial role for RB5 adsorption. The isotherm and kinetics adsorption models of RB5 removal by MMC-850 were Langmuir and Elovich, respectively. The intraparticle diffusion model suggested that RB5 adsorption onto MMC-850 was influenced by multisteps, film diffusion, and intraparticle diffusion. Thermodynamic studies described RB5 adsorption on MMC-850 as a spontaneous process and an exothermic adsorption process. The dominant mechanism of RB5 removal on MMC-850 was pore filling. MMC-850 is not only an effective adsorbent for RB5 removal, but it can also be easily regenerated through thermal regeneration.

Abbreviations

α: Initial rate constant (mg/g·min)
β: Desorption constant during any one experiment (mg/g)
γA: Is solution density
b: Constant related to the affinity between an adsorbent and adsorbate (L/mg)
C: Constant associated with the thickness of the boundary layer (mg/g)
Ce: Equilibrium concentrations (mg/L)
C_0: Initial concentrations (mg/L)
E: Free energy adsorption (kJ/Mol)
$Fe(NO_3)_3$: Iron (III) nitrate nonahydrate
ΔG°: Standard Gibb's free energy change
h: Initial rate constant (mg/g·min)
ΔH°: Standard enthalpy change (kJ/Mol)
IPD: Intraparticle diffusion
k_1: PFO rate constant (1/min)
k_2: PSO rate constant (g/mg·min)
k_p: Rate constant of the intraparticle diffusion model (mg/g·min$^{1/2}$)
K_c: Dimensionless that obtained by Langmuir constant
K_F: Freundlich constant (mg/g)/(mg/L)
K_{RD}: Constant related to the adsorption energy (mol^2/kJ^2)
MW_A: Molecular weight of RB5 (g/mol)
n: The intensity parameter
pH_{PZC}: Point of zero charge
q_e: The amounts of adsorbed RB5 at equilibrium (mg/g)
q_t: The amount of RB5 uptake at any time (mg/g)
q_{RD}: The adsorption capacity (mg/g)
Q^0_{max}: Maximum monolayer adsorption capacity (mg/g)
R: Gas constant (J/mol K)
RB5: Reactive black 5
S_{BET}: Specific surface area (m^2/g)
ΔS°: Standard entropy change (ΔS^0)
T: Temperature (K)
t: Time (min)
V_{micro}: Micropore volume (cm^3/g)
V_{meso}: Mesopore volume (cm^3/g)
V: Solution volume (L)
W: Weight of adsorbent (g).

Data Availability

The supporting data used to support the findings of this study are available from the corresponding author upon request.

Conflicts of Interest

The authors declare that they have no conflicts of interest.

Acknowledgments

The authors would like to acknowledge Dr. Chanchana Thanachayanont from National Center for Metal and Materials Technology Center (MTEC) who provided insight and expertise that greatly assisted the research. This research

work was partially supported by Chiang Mai University. The authors would also like to thank Assistant Professor Dr. Yothin Chimupala from the Department of Industrial Chemistry, Faculty of Science, Chiang Mai University, for comments that greatly improved the manuscript. This work was supported by the Industry Academia Partnership Programme-18/19, Royal Academy of Engineering and Office of the Higher Education Commission (IAPP18-19\119), and Thai Graduate Institute of Science and Technology (TGIST), National Science and Technology Development Agency (SCA-CO-2562-9657-TH).

References

[1] A. Boretti and L. Rosa, "Reassessing the projections of the World Water Development Report," *npj Clean Water*, vol. 2, no. 1, p. 2, 2019.

[2] M. A. Shaikh, "Water conservation in textile industry," *Pakistan Textile Journal*, vol. 58, pp. 48–51, 2009.

[3] K. K. Samanta, P. Pandit, P. Samanta, and S. Basak, "3 - Water consumption in textile processing and sustainable approaches for its conservation," in *Water in Textiles and Fashion*, S. S. Muthu, Ed., pp. 41–59, Woodhead Publishing, 2019.

[4] M. El Bouraie and W. S. El Din, "Biodegradation of reactive black 5 by _Aeromonas hydrophila_ strain isolated from dye-contaminated textile wastewater," *Sustainable Environment Research*, vol. 26, no. 5, pp. 209–216, 2016.

[5] D. Balarak, T. J. al-Musawi, I. A. Mohammed, and H. Abasizadeh, "The eradication of reactive black 5 dye liquid wastes using Azolla filiculoides aquatic fern as a good and an economical biosorption agent," *SN Applied Sciences*, vol. 2, no. 6, p. 1015, 2020.

[6] S. Sarkar, A. Banerjee, U. Halder, R. Biswas, and R. Bandopadhyay, "Degradation of synthetic azo dyes of textile industry: a sustainable approach using microbial enzymes," *Water Conservation Science and Engineering*, vol. 2, no. 4, pp. 121–131, 2017.

[7] F. M. D. Chequer, G. A. R. de Oliveira, E. R. A. Ferraz, J. Carvalho, M. V. B. Zanoni, and D. P. de Oliveir, "Textile dyes: dyeing process and environmental impact," *Eco-Friendly Textile Dyeing and Finishing*, vol. 6, pp. 151–176, 2013.

[8] T. Hadibarata, L. A. Adnan, A. R. M. Yusoff et al., "Microbial decolorization of an azo dye reactive black 5 using white-rot fungus Pleurotus eryngii F032," *Water, Air, & Soil Pollution*, vol. 224, no. 6, p. 1595, 2013.

[9] S. Dutta, B. Gupta, S. K. Srivastava, and A. K. Gupta, "Recent advances on the removal of dyes from wastewater using various adsorbents: a critical review," *Materials Advances*, vol. 2, no. 14, pp. 4497–4531, 2021.

[10] E. Guibal and J. Roussy, "Coagulation and flocculation of dye-containing solutions using a biopolymer (chitosan)," *Reactive and Functional Polymers*, vol. 67, no. 1, pp. 33–42, 2007.

[11] D. Morshedi, Z. Mohammadi, M. M. Akbar Boojar, and F. Aliakbari, "Using protein nanofibrils to remove azo dyes from aqueous solution by the coagulation process," *Colloids and Surfaces. B, Biointerfaces*, vol. 112, pp. 245–254, 2013.

[12] F. R. Furlan, L. G. de Melo da Silva, A. F. Morgado, A. A. U. de Souza, and S. M. A. Guelli Ulson de Souza, "Removal of reactive dyes from aqueous solutions using combined coagulation/flocculation and adsorption on activated carbon," *Resources, Conservation and Recycling*, vol. 54, no. 5, pp. 283–290, 2010.

[13] L. Semiz, "Removal of reactive black 5 from wastewater by membrane filtration," *Polymer Bulletin*, vol. 77, no. 6, pp. 3047–3059, 2020.

[14] H. R. Rashidi, N. M. N. Sulaiman, N. A. Hashim, C. R. C. Hassan, and M. R. Ramli, "Synthetic reactive dye wastewater treatment by using nano-membrane filtration," *Desalination and Water Treatment*, vol. 55, no. 1, pp. 86–95, 2015.

[15] P. Colindres, H. Yee-Madeira, and E. Reguera, "Removal of reactive black 5 from aqueous solution by ozone for water reuse in textile dyeing processes," *Desalination*, vol. 258, no. 1-3, pp. 154–158, 2010.

[16] M. S. Lucas and J. A. Peres, "Decolorization of the azo dye reactive black 5 by Fenton and photo-Fenton oxidation," *Dyes and Pigments*, vol. 71, no. 3, pp. 236–244, 2006.

[17] C. L. Hsueh, Y. H. Huang, C. C. Wang, and C. Y. Chen, "Degradation of azo dyes using low iron concentration of Fenton and Fenton-like system," *Chemosphere*, vol. 58, no. 10, pp. 1409–1414, 2005.

[18] T. Zhou, X. Lu, J. Wang, F. S. Wong, and Y. Li, "Rapid decolorization and mineralization of simulated textile wastewater in a heterogeneous Fenton like system with/without external energy," *Journal of Hazardous Materials*, vol. 165, no. 1-3, pp. 193–199, 2009.

[19] V. M. Vasconcelos, F. L. Ribeiro, F. L. Migliorini et al., "Electrochemical removal of reactive black 5 azo dye using non-commercial boron-doped diamond film anodes," *Electrochimica Acta*, vol. 178, pp. 484–493, 2015.

[20] E. Valadez-Renteria, J. Oliva, and V. Rodriguez-Gonzalez, "Photocatalytic materials immobilized on recycled supports and their role in the degradation of water contaminants: a timely review," *Science of the Total Environment*, vol. 807, Part 2, article 150820, 2022.

[21] M. Işik and D. T. Sponza, "Anaerobic/aerobic treatment of a simulated textile wastewater," *Separation and Purification Technology*, vol. 60, no. 1, pp. 64–72, 2008.

[22] D. T. Sponza and M. Işik, "Decolorization and azo dye degradation by anaerobic/aerobic sequential process," *Enzyme and Microbial Technology*, vol. 31, no. 1-2, pp. 102–110, 2002.

[23] S.-J. You and J.-Y. Teng, "Anaerobic decolorization bacteria for the treatment of azo dye in a sequential anaerobic and aerobic membrane bioreactor," *Journal of the Taiwan Institute of Chemical Engineers*, vol. 40, no. 5, pp. 500–504, 2009.

[24] O. Gulnaz, A. Kaya, and S. Dincer, "The reuse of dried activated sludge for adsorption of reactive dye," *Journal of Hazardous Materials*, vol. 134, no. 1-3, pp. 190–196, 2006.

[25] A. Khalid, M. Arshad, and D. E. Crowley, "Biodegradation potential of pure and mixed bacterial cultures for removal of 4-nitroaniline from textile dye wastewater," *Water Research*, vol. 43, no. 4, pp. 1110–1116, 2009.

[26] I. Ali and V. K. Gupta, "Advances in water treatment by adsorption technology," *Nature Protocols*, vol. 1, no. 6, pp. 2661–2667, 2006.

[27] S. De Gisi, G. Lofrano, M. Grassi, and M. Notarnicola, "Characteristics and adsorption capacities of low-cost sorbents for wastewater treatment: a review," *Sustainable Materials and Technologies*, vol. 9, pp. 10–40, 2016.

[28] O. S. Nille, A. S. Patil, R. D. Waghmare et al., "Chapter 11 - valorization of tea waste for multifaceted applications: a step toward green and sustainable development," in *Valorization of Agri-Food Wastes and by-Products*, R. Bhat, Ed., pp. 219–236, Academic Press, 2021.

[29] A. W. M. Ip, J. P. Barford, and G. McKay, "A comparative study on the kinetics and mechanisms of removal of reactive black 5 by adsorption onto activated carbons and bone char," *Chemical Engineering Journal*, vol. 157, no. 2-3, pp. 434–442, 2010.

[30] D. A. Giannakoudakis, G. Z. Kyzas, A. Avranas, and N. K. Lazaridis, "Multi-parametric adsorption effects of the reactive dye removal with commercial activated carbons," *Journal of Molecular Liquids*, vol. 213, pp. 381–389, 2016.

[31] Z. Eren and F. N. Acar, "Adsorption of reactive black 5 from an aqueous solution: equilibrium and kinetic studies," *Desalination*, vol. 194, no. 1-3, pp. 1–10, 2006.

[32] D. Patabandige, S. Wadumethrige, and S. Wanniarachchi, "H_3PO_4-activated sawdust and rice husk as effective decolorizers for textile wastewater containing reactive black 5," *International journal of Environmental Science and Technology*, vol. 16, no. 12, pp. 8375–8388, 2019.

[33] S. Wong, N. A. N. Yac'cob, N. Ngadi, O. Hassan, and I. M. Inuwa, "From pollutant to solution of wastewater pollution: synthesis of activated carbon from textile sludge for dye adsorption," *Chinese Journal of Chemical Engineering*, vol. 26, no. 4, pp. 870–878, 2018.

[34] M. W. Tze, M. K. Aroua, and M. Szlachta, "Palm Shell-based activated carbon for removing reactive black 5 dye: equilibrium and kinetics studies," *BioResources*, vol. 11, pp. 1432–1447, 2016.

[35] B. Heibati, S. Rodriguez-Couto, A. Amrane, M. Rafatullah, A. Hawari, and M. A. al-Ghouti, "Uptake of reactive black 5 by pumice and walnut activated carbon: chemistry and adsorption mechanisms," *Journal of Industrial and Engineering Chemistry*, vol. 20, no. 5, pp. 2939–2947, 2014.

[36] Y. Yi, Z. Huang, B. Lu et al., "Magnetic biochar for environmental remediation: a review," *Bioresource Technology*, vol. 298, article 122468, 2020.

[37] X. Li, C. Wang, J. Zhang, J. Liu, B. Liu, and G. Chen, "Preparation and application of magnetic biochar in water treatment: a critical review," *Science of the Total Environment*, vol. 711, article 134847, 2020.

[38] F. Fan, Z. Yang, H. Li, Z. Shi, and H. Kan, "Preparation and properties of hydrochars from macadamia nut shell via hydrothermal carbonization," *Royal Society Open Science*, vol. 5, no. 10, article 181126, 2018.

[39] P. Pengthamkeerati, T. Satapanajaru, and O. Singchan, "Sorption of reactive dye from aqueous solution on biomass fly ash," *Journal of Hazardous Materials*, vol. 153, no. 3, pp. 1149–1156, 2008.

[40] R. Wang, G. Lu, W. Qiao, and J. Yu, "Catalytic graphitization of coal-based carbon materials with light rare earth elements," *Langmuir*, vol. 32, no. 34, pp. 8583–8592, 2016.

[41] C. A. Igwegbe, S. N. Oba, C. O. Aniagor, A. G. Adeniyi, and J. O. Ighalo, "Adsorption of ciprofloxacin from water: a comprehensive review," *Journal of Industrial and Engineering Chemistry*, vol. 93, pp. 57–77, 2021.

[42] H. N. Tran, Y. F. Wang, S. J. You, and H. P. Chao, "Insights into the mechanism of cationic dye adsorption on activated charcoal: the importance of $\pi - \pi$ interactions," *Process Safety and Environmental Protection*, vol. 107, pp. 168–180, 2017.

[43] L. O. Cortat, N. C. Zanini, R. F. S. Barbosa, A. G. de Souza, D. S. Rosa, and D. R. Mulinari, "A sustainable perspective for macadamia nutshell residues revalorization by green composites development," *Journal of Polymers and the Environment*, vol. 29, no. 10, pp. 3210–3226, 2021.

[44] U. Samaksaman, W. Pattaraprakorn, A. Neramittagapong, and E. Kanchanatip, "Solid fuel production from macadamia nut shell: effect of hydrothermal carbonization conditions on fuel characteristics," *Biomass Conversion and Biorefinery*, 2021.

[45] Z. Li, Q. Liang, C. Yang, L. Zhang, B. Li, and D. Li, "Convenient preparation of nitrogen-doped activated carbon from macadamia nutshell and its application in supercapacitor," *Journal of Materials Science: Materials in Electronics*, vol. 28, no. 18, pp. 13880–13887, 2017.

[46] O. B. Nchoe, T. D. Ntuli, M. J. Klink, F. M. Mtunzi, and V. E. Pakade, "A comparative study of acid-treated, base-treated, and Fenton-like reagent- treated biomass for Cr(VI) sequestration from aqueous solutions," *Water Environment Research*, vol. 93, no. 3, pp. 370–383, 2021.

[47] G. E. J. Poinern, G. Senanayake, N. Shah, X. N. Thi-le, G. M. Parkinson, and D. Fawcett, "Adsorption of the aurocyanide, Au(CN)2- complex on granular activated carbons derived from macadamia nut shells - a preliminary study," *Minerals Engineering*, vol. 24, no. 15, pp. 1694–1702, 2011.

[48] S. Wongcharee, V. Aravinthan, and L. Erdei, "Mesoporous activated carbon-zeolite composite prepared from waste macadamia nut shell and synthetic faujasite," *Chinese Journal of Chemical Engineering*, vol. 27, no. 1, pp. 226–236, 2019.

[49] W. Cai, J. Wei, Z. Li, Y. Liu, J. Zhou, and B. Han, "Preparation of amino-functionalized magnetic biochar with excellent adsorption performance for Cr(VI) by a mild one-step hydrothermal method from peanut hull," *Colloids and Surfaces A: Physicochemical and Engineering Aspects*, vol. 563, pp. 102–111, 2019.

[50] Y. Liu, S. P. Sohi, S. Liu, J. Guan, J. Zhou, and J. Chen, "Adsorption and reductive degradation of Cr(VI) and TCE by a simply synthesized zero valent iron magnetic biochar," *Journal of Environmental Management*, vol. 235, pp. 276–281, 2019.

[51] J. Dong, L. Shen, S. Shan et al., "Optimizing magnetic functionalization conditions for efficient preparation of magnetic biochar and adsorption of Pb(II) from aqueous solution," *Science of the Total Environment*, vol. 806, Part 4, article 151442, 2022.

[52] X. Zhang, L. Lv, Y. Qin, M. Xu, X. Jia, and Z. Chen, "Removal of aqueous Cr(VI) by a magnetic biochar derived from *Melia azedarach* wood," *Bioresource Technology*, vol. 256, pp. 1–10, 2018.

[53] X. Yao, L. Ji, J. Guo et al., "Magnetic activated biochar nanocomposites derived from wakame and its application in methylene blue adsorption," *Bioresource Technology*, vol. 302, article 122842, 2020.

[54] P. Yin, L. Zhang, P. Sun et al., "Apium-derived biochar loaded with $MnFe_2O_4$@C for excellent low frequency electromagnetic wave absorption," *Ceramics International*, vol. 46, no. 9, pp. 13641–13650, 2020.

[55] H. N. Tran, S. J. You, A. Hosseini-Bandegharaei, and H. P. Chao, "Mistakes and inconsistencies regarding adsorption of contaminants from aqueous solutions: a critical review," *Water Research*, vol. 120, pp. 88–116, 2017.

[56] M. A. Al-Ghouti and D. A. Da'ana, "Guidelines for the use and interpretation of adsorption isotherm models: a review," *Journal of Hazardous Materials*, vol. 393, article 122383, 2020.

[57] K. Y. Foo and B. H. Hameed, "Insights into the modeling of adsorption isotherm systems," *Chemical Engineering Journal*, vol. 156, no. 1, pp. 2–10, 2010.

[58] I. Langmuir, "The constitution and fundamental properties of solids and liquids," *Journal of the Franklin Institute*, vol. 183, no. 1, pp. 102–105, 1917.

[59] H. M. F. Freundlich, "über die adsorption in losungen (adsorption in solution)," *Zeitschrift für Physikalische Chemie*, vol. 57, pp. 385–490, 1906.

[60] M. M. Dubinin, "The equation of the characteristic curve of activated charcoal," *Proceedings of the USSR Academy of Sciences*, vol. 55, pp. 327–329, 1947.

[61] Y.-S. Ho, J. Porter, and G. McKay, "Equilibrium isotherm studies for the sorption of divalent metal ions onto peat: copper, nickel and lead single component systems," *Water Air and Soil Pollution*, vol. 141, no. 1/4, pp. 1–33, 2002.

[62] Y.-S. Ho, "Review of second-order models for adsorption systems," *Journal of Hazardous Materials*, vol. 136, no. 3, pp. 681–689, 2006.

[63] J. Wang and X. Guo, "Adsorption kinetic models: physical meanings, applications, and solving methods," *Journal of Hazardous Materials*, vol. 390, article 122156, 2020.

[64] S. Chien and W. Clayton, "Application of Elovich equation to the kinetics of phosphate release and sorption in soils," *Soil Science Society of America Journal*, vol. 44, no. 2, pp. 265–268, 1980.

[65] V. Vimonses, S. Lei, B. Jin, C. W. K. Chow, and C. Saint, "Kinetic study and equilibrium isotherm analysis of Congo red adsorption by clay materials," *Chemical Engineering Journal*, vol. 148, no. 2-3, pp. 354–364, 2009.

[66] H. K. Boparai, M. Joseph, and D. M. O'Carroll, "Kinetics and thermodynamics of cadmium ion removal by adsorption onto nano zerovalent iron particles," *Journal of Hazardous Materials*, vol. 186, no. 1, pp. 458–465, 2011.

[67] E. I. Unuabonah, K. O. Adebowale, and B. I. Olu-Owolabi, "Kinetic and thermodynamic studies of the adsorption of lead (II) ions onto phosphate-modified kaolinite clay," *Journal of Hazardous Materials*, vol. 144, no. 1-2, pp. 386–395, 2007.

[68] V. Vadivelan and K. V. Kumar, "Equilibrium, kinetics, mechanism, and process design for the sorption of methylene blue onto rice husk," *Journal of Colloid and Interface Science*, vol. 286, no. 1, pp. 90–100, 2005.

[69] W. J. Weber and J. C. Morris, "Kinetics of adsorption on carbon from solution," *Journal of the Sanitary Engineering Division*, vol. 89, no. 2, pp. 31–59, 1963.

[70] Z. Alothman, "A review: fundamental aspects of silicate mesoporous materials," *Materials*, vol. 5, pp. 2874–2902, 2012.

[71] M. D. Donohue and G. L. Aranovich, "Classification of Gibbs adsorption isotherms," *Advances in Colloid and Interface Science*, vol. 76-77, pp. 137–152, 1998.

[72] A. Siyasukh, Y. Chimupala, and N. Tonanon, "Preparation of magnetic hierarchical porous carbon spheres with graphitic features for high methyl orange adsorption capacity," *Carbon*, vol. 134, pp. 207–221, 2018.

[73] W.-J. Liu, K. Tian, Y. R. He, H. Jiang, and H. Q. Yu, "High-yield harvest of nanofibers/mesoporous carbon composite by pyrolysis of waste biomass and its application for high durability electrochemical energy storage," *Environmental Science & Technology*, vol. 48, no. 23, pp. 13951–13959, 2014.

[74] X. Zhu, F. Qian, Y. Liu et al., "Controllable synthesis of magnetic carbon composites with high porosity and strong acid resistance from hydrochar for efficient removal of organic pollutants: an overlooked influence," *Carbon*, vol. 99, pp. 338–347, 2016.

[75] Z. Feng, R. Yuan, F. Wang, Z. Chen, B. Zhou, and H. Chen, "Preparation of magnetic biochar and its application in catalytic degradation of organic pollutants: a review," *Science of the Total Environment*, vol. 765, article 142673, 2020.

[76] X.-Y. Liu, M. Huang, H. L. Ma et al., "Preparation of a carbon-based solid acid catalyst by sulfonating activated carbon in a chemical reduction process," *Molecules*, vol. 15, no. 10, pp. 7188–7196, 2010.

[77] F. Fiorillo, C. Appino, and M. Pasquale, "Chapter 1 - Hysteresis in Magnetic Materials," in *The Science of Hysteresis*, pp. 1–190, 2006.

[78] A. M. Youssef, S. El-Khouly, and T. H. El-Nabarawy, "Removal of Pb (II) and cd (II) from aqueous solution using oxidized activated carbons developed from pecan shells," *Carbon Letters*, vol. 9, no. 1, pp. 8–16, 2008.

[79] B. Hayati and N. M. Mahmoodi, "Modification of activated carbon by the alkaline treatment to remove the dyes from wastewater: mechanism, isotherm and kinetic," *Desalination and Water Treatment*, vol. 47, no. 1-3, pp. 322–333, 2012.

[80] L. Zhou, H. Zhou, Y. Hu, S. Yan, and J. Yang, "Adsorption removal of cationic dyes from aqueous solutions using ceramic adsorbents prepared from industrial waste coal gangue," *Journal of Environmental Management*, vol. 234, pp. 245–252, 2019.

[81] M. Amin and P. Alazba, "Comparative study of the absorptive potential of raw and activated carbon Acacia nilotica for reactive black 5 dye," *Environmental Earth Sciences*, vol. 76, no. 16, p. 581, 2017.

[82] A. H. Nordin, S. Wong, N. Ngadi, M. Mohammad Zainol, N. A. F. Abd Latif, and W. Nabgan, "Surface functionalization of cellulose with polyethyleneimine and magnetic nanoparticles for efficient removal of anionic dye in wastewater," *Journal of Environmental Chemical Engineering*, vol. 9, no. 1, article 104639, 2021.

[83] M. Chang, Y. H. Shih, and Y.-H. Shih, "Synthesis and application of magnetic iron oxide nanoparticles on the removal of reactive black 5: reaction mechanism, temperature and pH effects," *Journal of Environmental Management*, vol. 224, pp. 235–242, 2018.

[84] F. Salvador, N. Martin-Sanchez, R. Sanchez-Hernandez, M. J. Sanchez-Montero, and C. Izquierdo, "Regeneration of carbonaceous adsorbents. Part I: thermal regeneration," *Microporous and Mesoporous Materials*, vol. 202, pp. 259–276, 2015.